Equivalent models of corrugated panels

Y. Xia [a], M.I. Friswell [a,*], E.I. Saavedra Flores [a,b]

[a] College of Engineering, Swansea University, Swansea SA2 8PP, UK
[b] Departamento de Ingeniería en Obras Civiles, Universidad de Santiago de Chile, Av. Ecuador 3659, Santiago, Chile

ARTICLE INFO

ABSTRACT

The design of corrugated panels has wide application in engineering. For example corrugated panels are often used in roof structures in civil engineering. More recently corrugated laminates have been suggested as a good solution for morphing aircraft skins due to their extremely anisotropic behaviour. The optimal design of these structures requires simple models of the panels or skins that may be incorporated into multi-disciplinary system models. Thus equivalent material models are required that retain the dependence on the geometric parameters of the corrugated skins or panels. An homogenisation-based analytical model, which could be used for any corrugation shape, is suggested in this paper. This method is based on a simplified geometry for a unit-cell and the stiffness properties of original sheet. This paper outlines such a modelling strategy, gives explicit expressions to calculate the equivalent material properties, and demonstrates the performance of the approach using two popular corrugation shapes.

© 2012 Elsevier Ltd. All rights reserved.

1. Introduction

Over the last two decades, homogenisation-based modelling techniques have attracted considerable attention within the computational mechanics community (Michel et al., 1999, 2002; Pellegrino et al., 1999; Suquet, 1993; Saavedra Flores and de Souza Neto, 2010). The importance and increasing interest in this area stems mainly from the potential ability of these techniques to capture the effective response of complex microstructural configurations under a wide range of conditions. Successful use of such methodologies has been reported, for example, in the context of constitutive modelling of materials (Miehe et al., 1999; Wellmann and Wriggers, 2008; Saavedra Flores et al., 2011), topology optimisation (Allaire, 2001; Bendsoe and Kikuchi, 1998) and waves propagation in periodic media (Ruzzene and Baz, 2000; Andrianov et al., 2008; Gonella and Ruzzene, 2008).

Many components in engineering structures incorporate corrugated panels, particularly in civil, marine and aerospace engineering. The response of these structures has to be estimated to ensure their performance is satisfactory. Often the loads are well distributed and only the overall deflections are required. If the dimensions of the whole corrugated panel are much larger than the period of the corrugations, then a suitable approach is the use of homogenisation techniques, in which the corrugated panel is replaced by an orthotropic plate with equivalent stiffness properties (Yokozeki et al., 2006; Thill et al., 2010a; Xia and Friswell, 2011).

Briassoulis (1986) and McFarland (1967) investigated the equivalent flexural rigidity of plates with sine-wave and rectangular corrugations, respectively. Samanta and Mukhopadhyay (1999) performed the static and dynamic analyses of trapezoidal corrugated sheets by considering both extensional and flexural rigidities. Yokozeki et al. (2006) investigated the properties of corrugated laminates made from carbon epoxy composites both by experiment and analysis. Peng et al. (2007) investigated the equivalent elastic properties of sinusoidal and trapezoidal corrugated plates by means of a mesh-free Galerkin method. Liew et al. (2007) used this method for the geometrically nonlinear analysis of corrugated plates. Both the equivalent flexural and extensional properties were employed in the analyses. Thill et al. (2008b, 2010b) compared the homogenised plate properties for candidate morphing aircraft skins to experimental results by adopting the same procedure proposed by Samanta and Mukhopadhyay (1999). Kress and Winkler (2010) and Winkler and Kress (2010) derived accurate analytical expressions of equivalent orthotropic plate for circular corrugations. Recently, a two-dimensional finite element was derived by Kress and Winkler (2011) for the analysis of corrugated laminates.

Recently morphing aircraft have attracted considerable interest (Barbarino et al., 2011). Mechanisms such as deployable flaps provide the current standard of adaptive airfoil geometry, although this solution places limitations on manoeuvrability and efficiency, and produces a design that is non-optimal in many flight regimes. Although significant efforts have been expended in research into adaptive structures and morphing aircraft, examples of practical solutions are still very few. One important issue that remains to be solved is the design of the suitable skins (Thill et al., 2008a).

* Corresponding author. Tel.: +44 (0)1792 602969; fax: +44 (0)1792 295157.
  E-mail address: m.i.friswell@swansea.ac.uk (M.I. Friswell).

Corrugated laminates offer a solution due to their extremely anisotropic behaviour: compliance in the chordwise (corrugation) direction that allows shape changes and increases in surface area; stiffness in the spanwise (transverse to the corrugation) direction enables the aerodynamic and inertial loads to be carried. Currently the design of the morphing wing and the specification of the skin are performed independently. This approach is adequate for simple wing geometries (such as morphing trailing edges), but inadequate for more complex three-dimensional geometries (such as the morphing winglet (Smith et al., 2010)).

This paper investigates equivalent material models that reduce the size of the finite element models, so that the panel or skin may be incorporated into the system level model. The skin model must retain dependence on the geometric parameters of the corrugations so that it may be used for optimisation at the design stage. Furthermore the method must allow for the geometry of arbitrary corrugations to be modelled and analysed easily. This paper proposes an homogenisation method that is more accurate and versatile than existing methods. Both the in-plane and the out-of-plane local deformations of the sheet material are considered. The homogenisation-based analytical model is obtained from a simplified geometry for a unit-cell and the validity of this model is compared to a detailed finite element analysis. The proposed method is easily applied to any corrugation geometry, through the evaluation of two integrals based solely on the geometry; often these integrals may be evaluated analytically but in some instances might have to be calculated numerically. The approach is demonstrated on two common geometries, namely trapezoidal and round corrugations; other corrugation shapes are easily analysed.

2. Modelling corrugated panels

The panel is assumed to have periodic corrugations in one direction only. Our objective is to approximate the response of the corrugated panel using an orthotropic flat plate whose properties are selected to be equivalent to those of the original panel. The same boundary conditions are applied to the equivalent orthotropic plate and to the original corrugated panel, and the homogenised properties are estimated by equating the strain energies and the reaction forces and moments from the two models.

2.1. Coordinate systems

The corrugated panels are generated from a periodic shape in the xz plane that is extruded in the y direction to produce a panel.
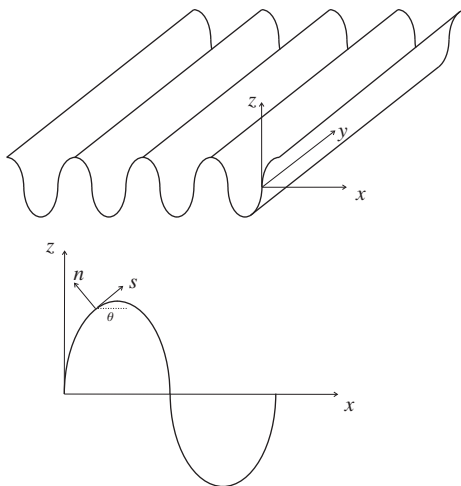

Fig. 1. Definition of the coordinate systems.

The geometry of a corrugation unit is shown in Fig. 1. There are two coordinate systems that must be defined to analyse the panel, namely the global xyz Cartesian coordinate system as shown in Fig. 1, and the local coordinate system on the sheet forming the corrugation. The local coordinate system is defined by the tangent direction to the sheet in the xz plane, defined as the s direction, and the normal to the sheet in the xz plane, defined as the n direction. Both of these directions are shown in Fig. 1. We define the position of a point on the sheet, $\mathbf{r} \equiv \mathbf{r}(s, y)$, in the global coordinate system as

$$\mathbf{r}(s, y) = x(s)\mathbf{i} + y\mathbf{j} + z(s)\mathbf{k}, \tag{1}$$

where $\mathbf{i}, \mathbf{j}$ and $\mathbf{k}$ denote unit vectors in the x, y and z directions, respectively, and s defines the position along the corrugation. The unit vectors in the local coordinate system, $\mathbf{e_t}$ and $\mathbf{e_n}$, tangent and normal to the corrugation in the xz plane, are defined as

$$\mathbf{e_t} = \frac{d\mathbf{r}}{ds} = \cos\theta\mathbf{i} + \sin\theta\mathbf{k} \tag{2}$$

and

$$\mathbf{e_n} = \sin\theta\mathbf{i} - \cos\theta\mathbf{k}, \tag{3}$$

where $\cos\theta$ denotes the direction cosine of the tangential direction, given by

$$\cos\theta = \frac{dx}{ds}, \quad \sin\theta = \frac{dz}{ds}. \tag{4}$$

It is assumed that the principal directions of the orthotropic sheet material forming the corrugations coincide with the coordinates y and s of the plate, and as shall be seen in the following, this assumption will allow us to set most of the terms in the stiffness matrices to zero. Thus, the results obtained here should be restricted to this particular case of orthotropy. However, the consideration of different directions of material is straightforward and if required may be included in the present methodology.

2.2. Equivalent orthotropic plate model

The corrugated panel is approximated by an orthotropic classical Kirchhoff plate, by ignoring the coupling stiffness matrix $\mathbf{B}$. The constitutive equation of the equivalent orthotropic plate is

$$\begin{Bmatrix} \overline{N}_x \\ \overline{N}_y \\ \overline{N}_{xy} \\ \overline{M}_x \\ \overline{M}_y \\ \overline{M}_{xy} \end{Bmatrix} = \begin{bmatrix} \overline{A}_{11} & \overline{A}_{12} & 0 & 0 & 0 & 0 \\ \overline{A}_{12} & \overline{A}_{22} & 0 & 0 & 0 & 0 \\ 0 & 0 & \overline{A}_{66} & 0 & 0 & 0 \\ 0 & 0 & 0 & \overline{D}_{11} & \overline{D}_{12} & 0 \\ 0 & 0 & 0 & \overline{D}_{12} & \overline{D}_{22} & 0 \\ 0 & 0 & 0 & 0 & 0 & \overline{D}_{66} \end{bmatrix} \begin{Bmatrix} \bar{\epsilon}_x \\ \bar{\epsilon}_y \\ \bar{\gamma}_{xy} \\ \bar{\kappa}_x \\ \bar{\kappa}_y \\ \bar{\kappa}_{xy} \end{Bmatrix}, \tag{5}$$

where $\bar{\epsilon}_x, \bar{\epsilon}_y, \bar{\gamma}_{xy}, \bar{\kappa}_x, \bar{\kappa}_y, \bar{\kappa}_{xy}$ denote the strain components and curvature components of the mid-plane of the orthotropic plate model, and $\overline{N}_x, \overline{N}_y, \overline{N}_{xy}, \overline{M}_x, \overline{M}_y, \overline{M}_{xy}$ denote the force and moment components. Eq. (5) may be written in a compact but equivalent form as

$$\begin{Bmatrix} \overline{\mathbf{N}} \\ \overline{\mathbf{M}} \end{Bmatrix} = \begin{bmatrix} \overline{\mathbf{A}} & \mathbf{0} \\ \mathbf{0} & \overline{\mathbf{D}} \end{bmatrix} \begin{Bmatrix} \bar{\boldsymbol{\epsilon}} \\ \bar{\boldsymbol{\kappa}} \end{Bmatrix}, \tag{6}$$

where the definition of the vectors and matrices is obvious by comparing Eqs. (5) and (6).

The objective is to derive closed form approximate expressions of the $\overline{A}_{ij}$ and $\overline{D}_{ij}$ terms in Eq. (5) as a function of the corrugation geometry.

2.3. Evaluation of the stiffness properties

As the corrugated panel is formed by repeating the basic unit cell periodically, the stiffness properties of the equivalent plate may be determined from a basic unit cell, called a Representative Volume Element (RVE). In the local curvilinear coordinates (s, n, y), we have,

$$
\begin{Bmatrix} N_s \\ N_y \\ N_{sy} \\ M_s \\ M_y \\ M_{sy} \end{Bmatrix} = \begin{bmatrix} A_{11} & A_{12} & 0 & 0 & 0 & 0 \\ A_{12} & A_{22} & 0 & 0 & 0 & 0 \\ 0 & 0 & A_{66} & 0 & 0 & 0 \\ 0 & 0 & 0 & D_{11} & D_{12} & 0 \\ 0 & 0 & 0 & D_{12} & D_{22} & 0 \\ 0 & 0 & 0 & 0 & 0 & D_{66} \end{bmatrix} \begin{Bmatrix} \epsilon_s \\ \epsilon_y \\ \gamma_{sy} \\ \kappa_s \\ \kappa_y \\ \kappa_{sy} \end{Bmatrix}. \tag{7}
$$

The homogenisation approach requires the estimation of the internal force distributions under six generalised strain boundary conditions for $\left\{ \begin{smallmatrix} \bar{\epsilon} \\ \bar{\kappa} \end{smallmatrix} \right\}$ which are shown in Table 1. Either the Equivalent Energy Method or the Equivalent Force Method may be used to estimate the equivalent stiffnesses of the corrugated panels; the energy approach is generally simpler, but is only able to estimate the diagonal terms in Eq. (5).

For the Equivalent Energy Method, the strain energy of the original corrugated panel is calculated as

$$
U = \frac{1}{2} \iint \mathbf{N}^\top \mathbf{S} \mathbf{N} \, ds \, dy, \tag{8}
$$

where $\mathbf{N} = [N_s, N_y, N_{sy}, M_s, M_y, M_{sy}]^T$. The flexibility matrix of the original plain composite sheet material, $\mathbf{S}$, is the inverse of the stiffness matrix, $\mathbf{K}$ (the matrix in Eq. (7)), and given by

$$
\mathbf{S} = \mathbf{K}^{-1} = \begin{bmatrix} S_{11} & S_{12} & 0 & 0 & 0 & 0 \\ S_{12} & S_{22} & 0 & 0 & 0 & 0 \\ 0 & 0 & S_{33} & 0 & 0 & 0 \\ 0 & 0 & 0 & S_{44} & S_{45} & 0 \\ 0 & 0 & 0 & S_{45} & S_{55} & 0 \\ 0 & 0 & 0 & 0 & 0 & S_{66} \end{bmatrix} \tag{9}
$$

where,

$$
S_{11} = \frac{A_{22}}{A_{11}A_{22} - A_{12}^2}, \quad S_{12} = \frac{-A_{12}}{A_{11}A_{22} - A_{12}^2},
$$

$$
S_{22} = \frac{A_{11}}{A_{11}A_{22} - A_{12}^2}, \quad S_{33} = \frac{1}{A_{66}},
$$

$$
S_{44} = \frac{D_{22}}{D_{11}D_{22} - D_{12}^2}, \quad S_{45} = \frac{-D_{12}}{D_{11}D_{22} - D_{12}^2},
$$

$$
S_{55} = \frac{D_{11}}{D_{11}D_{22} - D_{12}^2}, \quad S_{66} = \frac{1}{D_{66}}.
$$

The integration in Eq. (8) is over a unit cell whose length corresponds to one period of the corrugation and the width is b.

Table 1
Boundary conditions for the equivalent orthotropic plate, and the corresponding stiffness expressions.

Boundary conditions $\left\{ \begin{smallmatrix} \bar{\epsilon} \\ \bar{\kappa} \end{smallmatrix} \right\}$	Equivalent energy method	Equivalent force method
$[1,0,0,0,0,0]^T$	$\bar{A}_{11} = 2U/(2cb)$	$\bar{A}_{11} = \bar{N}_x; \; \bar{A}_{21} = \bar{N}_y$
$[0,1,0,0,0,0]^T$	$\bar{A}_{22} = 2U/(2cb)$	$\bar{A}_{22} = \bar{N}_y; \; \bar{A}_{12} = \bar{N}_x$
$[0,0,1,0,0,0]^T$	$\bar{A}_{66} = 2U/(2cb)$	$\bar{A}_{66} = \bar{N}_{xy}$
$[0,0,0,1,0,0]^T$	$\bar{D}_{11} = 2U/(2cb)$	$\bar{D}_{11} = \bar{M}_x; \; \bar{D}_{21} = \bar{M}_y$
$[0,0,0,0,1,0]^T$	$\bar{D}_{22} = 2U/(2cb)$	$\bar{D}_{22} = \bar{M}_y; \; \bar{D}_{21} = \bar{M}_x$
$[0,0,0,0,0,1]^T$	$\bar{D}_{66} = 2U/(2cb)$	$\bar{D}_{66} = \bar{M}_{xy}$

The strain energy, U, must equal the strain energy of the equivalent orthotropic plate, $\bar{U}$. Hence

$$
U = \bar{U} = \frac{1}{2}(2c)b \begin{Bmatrix} \bar{\epsilon} \\ \bar{\kappa} \end{Bmatrix}^T \begin{bmatrix} \bar{\mathbf{A}} & \mathbf{0} \\ \mathbf{0} & \bar{\mathbf{D}} \end{bmatrix} \begin{Bmatrix} \bar{\epsilon} \\ \bar{\kappa} \end{Bmatrix}, \tag{10}
$$

where $2c$ is the period of the corrugation and b is the width of the unit cell. The stiffness components are then estimated by applying different strain boundary conditions in turn. The equivalent stiffness component expressions and corresponding boundary conditions are shown in Table 1.

The Equivalent Force Method equates the equivalent internal forces and moments to the *average* internal forces and moments of the original corrugated RVE for the six different strain boundary conditions shown in Table 1. Different stiffness components are obtained from an appropriate choice of equivalent internal force and prescribed strain boundary condition. The details are also shown in Table 1.

The following subsections explain how each of stiffness components is calculated by using the six strain boundary conditions. The development for the first boundary condition is explained in detail; the development for the other boundary conditions is similar and hence only a brief summary is given.

2.3.1. Case 1: $[\bar{\epsilon}^T, \bar{\kappa}^T] = [1, 0, 0, 0, 0, 0]$

From Table 1, we have $\bar{N}_x = \bar{A}_{11}$. The symmetry of the corrugations and the boundary conditions require that most of the local strains are zero; thus $\epsilon_y = 0, \gamma_{sy} = 0, \kappa_y = 0$ and $\kappa_{sy} = 0$. Since the only strain is in the x direction, the internal force in the x direction for the corrugated sheet must be constant, and hence the equilibrium of internal forces in the local coordinate system implies that

$$
N_s = \bar{N}_x \frac{dx}{ds}. \tag{11}
$$

The zero strain in the y direction in the local coordinates requires that

$$
N_y = \frac{A_{12}}{A_{11}}, \quad N_s = \frac{A_{12}}{A_{11}}, \quad \bar{N}_x \frac{dx}{ds}. \tag{12}
$$

Comparing moments between the local and global coordinates systems gives

$$
M_s = \bar{N}_x z \tag{13}
$$

and zero local curvature gives

$$
M_y = \frac{D_{12}}{D_{11}}, \quad M_s = \frac{D_{12}}{D_{11}} \bar{N}_x z. \tag{14}
$$

Thus the strain energy of the RVE is

$$
U = \frac{1}{2} \iint_A \left(N_s^2 S_{11} + 2N_s N_y S_{12} + N_y^2 S_{22} + M_s^2 S_{44} + 2M_s M_y S_{45} + M_y^2 S_{55} \right) ds \, dy
$$

$$
= \frac{1}{2} \int_0^b \int_s \bar{N}_x^2 \left[\left(\frac{dx}{ds} \right)^2 \left(S_{11} + 2\frac{A_{12}}{A_{11}} S_{12} + \frac{A_{12}^2}{A_{11}^2} S_{22} \right) \right.
$$

$$
\left. + z^2 \left(S_{44} + 2\frac{D_{12}}{D_{11}} S_{45} + \frac{D_{12}^2}{D_{11}^2} S_{55} \right) \right] ds \, dy
$$

$$
= \frac{1}{2} b \bar{A}_{11}^2 \int_s \left[\left(\frac{dx}{ds} \right)^2 \left(S_{11} + 2\frac{A_{12}}{A_{11}} S_{12} + \frac{A_{12}^2}{A_{11}^2} S_{22} \right) \right.
$$

$$
\left. + z^2 \left(S_{44} + 2\frac{D_{12}}{D_{11}} S_{45} + \frac{D_{12}^2}{D_{11}^2} S_{55} \right) \right] ds. \tag{15}
$$

Using the definitions in Eq. (9),

$$
\left(S_{11} + 2\frac{A_{12}}{A_{11}} S_{12} + \frac{A_{12}^2}{A_{11}^2} S_{22} \right) = \frac{1}{A_{11}} \tag{16}
$$

and

$$\left(S_{44} + 2\frac{D_{12}}{D_{11}}S_{45} + \frac{D_{12}^2}{D_{11}^2}S_{55}\right) = \frac{1}{D_{11}}. \tag{17}$$

Hence

$$U = \frac{1}{2}b\overline{A}_{11}^2 \int_s \left[\left(\frac{dx}{ds}\right)^2 \frac{1}{A_{11}} + z^2 \frac{1}{D_{11}}\right]ds = \frac{1}{2}b\overline{A}_{11}^2\left[\frac{I_1}{A_{11}} + \frac{I_2}{D_{11}}\right], \tag{18}$$

where

$$I_1 = \int_s \left(\frac{dx}{ds}\right)^2 ds \quad \text{and} \quad I_2 = \int_s z^2 ds. \tag{19}$$

The strain energy of the equivalent panel, $\overline{U}$, is

$$\overline{U} = \frac{1}{2}(2c)b\overline{A}_{11} = bc\overline{A}_{11}. \tag{20}$$

Since $\overline{U} = U$, we have

$$\overline{A}_{11} = \frac{2c}{\frac{I_1}{A_{11}} + \frac{I_2}{D_{11}}}. \tag{21}$$

Note that the geometry of the corrugations only affect I_1 and I_2 since $(x(s), z(s))$ defines the shape of the corrugations.

The equivalent internal force, $\overline{N}_y$, is obtained as the average local force, N_y, over a corrugation. Thus

$$\overline{N}_y = \frac{1}{2c}\int_s N_y ds = \frac{1}{2c}\int_s \frac{A_{12}}{A_{11}}\overline{N}_x\frac{dx}{ds}ds$$
$$= \frac{1}{2c}\frac{A_{12}}{A_{11}}\overline{A}_{11}\int_0^{2c}dx = \frac{A_{12}}{A_{11}}\overline{A}_{11}. \tag{22}$$

The coupling stiffness components $\overline{A}_{21}$ and $\overline{A}_{12}$ are then

$$\overline{A}_{12} = \overline{A}_{21} = \overline{N}_y = \frac{A_{12}}{A_{11}}\overline{A}_{11} \tag{23}$$

and the Poisson's ratio of the equivalent plate is identical to that of the sheet material used to form the corrugations.

2.3.2. Case 2: $[\bar{\epsilon}^T, \bar{\kappa}^T] = [0, 1, 0, 0, 0, 0]$

In this case, $\overline{N}_x = \overline{A}_{12}$ and $\overline{N}_y = \overline{A}_{22}$. The local strains are given by $\epsilon_y = 1, \gamma_{sy} = 0, \kappa_y = 0$ and $\kappa_{sy} = 0$. Equating forces in the local coordinate system gives

$$N_s = \overline{N}_x\frac{dx}{ds} = \overline{A}_{12}\frac{dx}{ds}. \tag{24}$$

From Eq. (7), $N_s = A_{11}\epsilon_s + A_{12}\epsilon_y$, and hence

$$\epsilon_s = \frac{1}{A_{11}}\left(\overline{A}_{12}\frac{dx}{ds} - A_{12}\right). \tag{25}$$

From the definition of N_y in Eq. (7), and substituting for ϵ_s from Eq. (25), gives

$$N_y = A_{12}\epsilon_s + A_{22} = \frac{\overline{A}_{12}A_{12}}{A_{11}}\frac{dx}{ds} + \left(A_{22} - \frac{A_{12}^2}{A_{11}}\right). \tag{26}$$

The average internal force in the global frame, $\overline{N}_y$, is then

$$\overline{N}_y = \frac{1}{2c}\int_s N_y ds$$
$$= \frac{1}{2c}\left[\int_s \left(\frac{\overline{A}_{12}A_{12}}{A_{11}}\frac{dx}{ds}\right)ds + \int_s \frac{A_{11}A_{22} - A_{12}^2}{A_{11}}ds\right]$$
$$= \frac{\overline{A}_{12}A_{12}}{A_{11}} + \frac{l}{c}\frac{A_{11}A_{22} - A_{12}^2}{A_{11}}, \tag{27}$$

where l is the developed length of one half of a repeating corrugation. The constant $\overline{A}_{22}$ is then obtained as

$$\overline{A}_{22} = \overline{N}_y = \frac{\overline{A}_{12}A_{12}}{A_{11}} + \frac{l}{c}\frac{A_{11}A_{22} - A_{12}^2}{A_{11}}. \tag{28}$$

The effect of different corrugation geometries only affects $\overline{A}_{22}$ through the length l.

2.3.3. Case 3: $[\bar{\epsilon}^T, \bar{\kappa}^T] = [0, 0, 1, 0, 0, 0]$

In this case, we have $N_{sy} = \overline{N}_{xy} = \overline{A}_{66}$. The strain energy of the RVE is,

$$U = \frac{1}{2}\iint_A N_{sy}^2 S_{33}dsdy = \frac{1}{2}b(2l)\overline{A}_{66}^2 S_{33}. \tag{29}$$

Equating this strain energy to the strain energy for the equivalent plate model gives

$$U = \overline{U} = \frac{1}{2}b(2c)\overline{A}_{66} = bc\overline{A}_{66}. \tag{30}$$

Thus,

$$\overline{A}_{66} = \frac{c}{lS_{33}} = \frac{c}{l}A_{66}. \tag{31}$$

The effect of different corrugation geometries only affects $\overline{A}_{66}$ through the length l.

2.3.4. Case 4: $[\bar{\epsilon}^T, \bar{\kappa}^T] = [0, 0, 0, 1, 0, 0]$

In this case, $\overline{M}_x = \overline{D}_{11}$ and $\overline{M}_y = \overline{D}_{21}$. The local strains are given by $\epsilon_s = 0, \epsilon_y = 0, \gamma_{sy} = 0, \kappa_y = 0$ and $\kappa_{sy} = 0$. Thus,

$$M_s = \overline{M}_x \tag{32}$$

and

$$M_y = \frac{D_{12}}{D_{11}}M_s = \frac{D_{12}}{D_{11}}\overline{M}_x. \tag{33}$$

The strain energy of the RVE is

$$U = \frac{1}{2}\iint_A \left(M_s^2 S_{44} + 2M_s M_y S_{45} + M_y^2 S_{55}\right)dsdy$$
$$= \frac{1}{2}\int_0^b \int_s \overline{M}_x^2\left(S_{44} + 2\frac{D_{12}}{D_{11}}S_{45} + \frac{D_{12}^2}{D_{11}^2}S_{55}\right)dsdy$$
$$= \frac{1}{2}b(2l)\overline{D}_{11}^2\left(S_{44} + 2\frac{D_{12}}{D_{11}}S_{45} + \frac{D_{12}^2}{D_{11}^2}S_{55}\right) = \frac{1}{2}b(2l)\overline{D}_{11}^2\frac{1}{D_{11}}. \tag{34}$$

The strain energy of the equivalent plate, $\overline{U}$, is

$$\overline{U} = \frac{1}{2}\overline{D}_{11}b(2c). \tag{35}$$

Equating the strain energies, $\overline{U} = U$, we have,

$$\overline{D}_{11} = \frac{c}{l}D_{11}. \tag{36}$$

The coupling bending stiffness components, $\overline{D}_{12}$ and $\overline{D}_{21}$, are calculated as follows,

$$\overline{D}_{12} = \overline{D}_{21} = \overline{M}_y = \frac{1}{2c}\int_s M_y\frac{dx}{ds}ds$$
$$= \frac{1}{2c}\int_s \frac{D_{12}}{D_{11}}\overline{D}_{11}\frac{dx}{ds}ds$$
$$= \frac{1}{2c}\frac{D_{12}}{D_{11}}\overline{D}_{11}\int_0^{2c}dx = \frac{D_{12}}{D_{11}}\overline{D}_{11}. \tag{37}$$

2.3.5. Case 5: $[\bar{\epsilon}^T, \bar{\kappa}^T] = [0, 0, 0, 0, 1, 0]$

In this case, the local strains are given by $\epsilon_s = 0, \epsilon_y = z, \gamma_{sy} = 0, \kappa_s = 0, \kappa_s = 0, \kappa_y = dx/ds, \kappa_{sy} = 0$. The strain energy of the RVE is then

Table 2
Stiffness properties for a general corrugation, with half period c and half length l.

Stiffness term	Expression from proposed method
$\bar{A}_{11}$	$\dfrac{2c}{\left[\dfrac{I_1}{A_{11}}+\dfrac{I_2}{D_{11}}\right]}$
$\bar{A}_{12}$	$\dfrac{A_{12}}{A_{11}}\bar{A}_{11}$
$\bar{A}_{22}$	$\dfrac{\bar{A}_{12}A_{12}}{A_{11}}+\dfrac{l}{c}\dfrac{A_{11}A_{22}-A_{12}^2}{A_{11}}$
$\bar{A}_{66}$	$\dfrac{c}{l}A_{66}$
$\bar{D}_{11}$	$\dfrac{c}{l}D_{11}$
$\bar{D}_{12}$	$\dfrac{D_{12}}{D_{11}}\bar{D}_{11}$
$\bar{D}_{22}$	$\dfrac{1}{2c}[I_2A_{22}+I_1D_{22}]$
$\bar{D}_{66}$	$\dfrac{l}{c}D_{66}$

where $I_1=\int_0^{2l}\left(\dfrac{dx}{ds}\right)^2 ds$ and $I_2=\int_0^{2l} z^2 ds$.

$$U=\frac{1}{2}\iint_A\left[A_{22}z^2+D_{22}\left(\frac{dx}{ds}\right)^2\right]dsdy$$
$$=\frac{1}{2}b\int_s\left[A_{22}z^2+D_{22}\left(\frac{dx}{ds}\right)^2\right]ds. \tag{38}$$

The equivalent strain energy $\bar{U}$ is

$$\bar{U}=\frac{1}{2}b(2c)\bar{D}_{22}. \tag{39}$$

Hence $\bar{U}=U$ implies that

$$\bar{D}_{22}=\frac{1}{2c}\int_s\left[A_{22}z^2+D_{22}\left(\frac{dx}{ds}\right)^2\right]ds=\frac{1}{2c}[A_{22}I_2+D_{22}I_1], \tag{40}$$

where the integrals I_1 and I_2 are given in Eq. (19).

2.3.6. Case 6: $[\bar{\epsilon}^T,\bar{\kappa}^T]=[0,0,0,0,0,1]$

In this case, the local strains are $\epsilon_s=0, \epsilon_y=0, \gamma_{sy}=0, \kappa_s=0, \kappa_s=0, \kappa_y=0, \kappa_{sy}=1$. The strain energy of the RVE is then

$$U=\frac{1}{2}\iint_A D_{66}dsdy=\frac{1}{2}b(2l)D_{66}. \tag{41}$$

The equivalent strain energy, $\bar{U}$, is

$$\bar{U}=\frac{1}{2}b(2c)\bar{D}_{66}. \tag{42}$$

Hence $\bar{U}=U$ implies that

$$\bar{D}_{66}=\frac{l}{c}D_{66}. \tag{43}$$
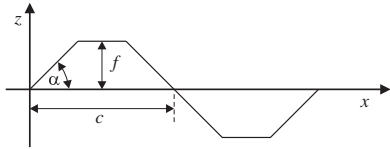
2.3.7. Summary of stiffness terms

Table 2 summarises the stiffness terms for a general corrugation defined by $(x(s),z(s))$. The constants that must be calculated for a given corrugation geometry are the half period c, the corrugation half length l, and the integrals I_1 and I_2.

3. Mechanical properties of typical corrugations

Using the method presented in Subsection 2.3, the stiffness properties of two classical corrugation shapes are estimated.

Table 3 gives the results for a trapezoidal corrugation. The corrugation half length is calculated by summing the lengths of the sloping and horizontal sections and is given by $l=\frac{2f}{\sin\alpha}+c-\frac{2f}{\tan\alpha}$. The integrals I_1 and I_2 are easily computed using the expressions in Table 2, and are given in Table 3. The proposed method is com-
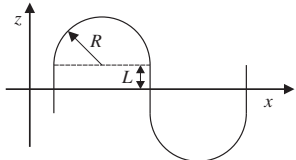
Table 3
Stiffness properties for a trapezoidal corrugation. Note that the corrugation half length is $l=\frac{2f}{\sin\alpha}+c-\frac{2f}{\tan\alpha}$. The method of Samanta and Mukhopadhyay (1999) assumes an isotropic sheet with thickness t, Young's modulus E, and Poisson's ratio v.

Stiffness Term	Proposed Method	Samanta and Mukhopadhyay (1999)
$\bar{A}_{11}$	$\dfrac{2c}{\left[\dfrac{I_1}{A_{11}}+\dfrac{I_2}{D_{11}}\right]}$	$\dfrac{2c}{I_2}\dfrac{Et^3}{12}$
$\bar{A}_{12}$	$\dfrac{A_{12}}{A_{11}}\bar{A}_{11}$	$v\bar{A}_{11}$
$\bar{A}_{22}$	$\dfrac{\bar{A}_{12}A_{12}}{A_{11}}+\dfrac{l}{c}\dfrac{A_{11}A_{22}-A_{12}^2}{A_{11}}$	$\dfrac{l}{c}Et$
$\bar{A}_{66}$	$\dfrac{c}{l}A_{66}$	$\dfrac{c}{l}\dfrac{Et}{2(1+v)}$
$\bar{D}_{11}$	$\dfrac{c}{l}D_{11}$	$\dfrac{c}{l}\dfrac{Et^3}{12}$
$\bar{D}_{12}$	$\dfrac{D_{12}}{D_{11}}\bar{D}_{11}$	0
$\bar{D}_{22}$	$\dfrac{1}{2c}[I_2A_{22}+I_1D_{22}]$	$\dfrac{Et}{2c}I_2$
$\bar{D}_{66}$	$\dfrac{l}{c}D_{66}$	$\dfrac{l}{c}\dfrac{Et^3}{6(1+v)}$

where $I_1=\dfrac{4f\cos\alpha}{3\sin\alpha}+2c-\dfrac{4f}{\tan\alpha}$, and $I_2=\dfrac{4f^3}{3\sin\alpha}+2f^2\left(c-\dfrac{2f}{\tan\alpha}\right)$

Table 4
Stiffness properties for a round corrugation. Note that the corrugation half length is $l=\pi R+2L$ and the half period is $c=2R$. The thickness of the corrugated sheet material is t.

Stiffness Term	Proposed Method	Yokozeki et al. (2006)
$\bar{A}_{11}$	$\dfrac{2c}{\left[\dfrac{I_1}{A_{11}}+\dfrac{I_2}{D_{11}}\right]}$	$\dfrac{4RD_{11}}{I_2}$
$\bar{A}_{12}$	$\dfrac{A_{12}}{A_{11}}\bar{A}_{11}$	
$\bar{A}_{22}$	$\dfrac{\bar{A}_{12}A_{12}}{A_{11}}+\dfrac{A_{11}A_{22}-A_{12}^2}{A_{11}}\dfrac{l}{2R}$	$\dfrac{l}{2R}A_{22}$
$\bar{A}_{66}$	$\dfrac{2R}{l}A_{66}$	
$\bar{D}_{11}$	$\dfrac{2R}{l}D_{11}$	$\dfrac{2R}{l}D_{11}$
$\bar{D}_{12}$	$\dfrac{D_{12}}{D_{11}}\bar{D}_{11}$	
$\bar{D}_{22}$	$\dfrac{1}{2c}[I_2A_{22}+I_1D_{22}]$	$\left[I_2+\dfrac{(3\pi R+8L)}{12}t^2\right]\dfrac{A_{22}}{4R}$
$\bar{D}_{66}$	$\dfrac{l}{2R}D_{66}$	

where $I_1=\pi R$, and $I_2=\dfrac{4L^3}{3}+2\pi L^2R+8LR^2+\pi R^3$

pared to that of Samanta and Mukhopadhyay (1999), who only considered isotropic material for the original sheet.

Table 4 gives the stiffness results for a round corrugation and are compared to the method of Yokozeki et al. (2006). The length is easily calculated as $l=\pi R+2L$. The integrals I_1 and I_2 are given in Table 4.

Table 5
Stiffness properties for the example trapezoidal corrugation.

	Proposed method	Samanta and Mukhopadhyay (1999)	FEM	Error (%) Proposed method vs. FEM
$\overline{A}_{11}$ (MN/m)	4.052	4.150	4.051	0.012
$\overline{A}_{12}$ (MN/m)	1.216	1.245	1.215	0.008
$\overline{A}_{22}$ (MN/m)	161.332	176.888	163.910	1.572
$\overline{A}_{66}$ (MN/m)	42.489	42.489	42.797	0.721
$\overline{D}_{11}$ (Nm)	407.917	371.205	406.512	0.346
$\overline{D}_{12}$ (Nm)	122.375	0	121.954	0.349
$\overline{D}_{22}$ (kNm)	17.809	31.647	17.805	0.020
$\overline{D}_{66}$ (Nm)	208.032	208.032	207.96	0.035
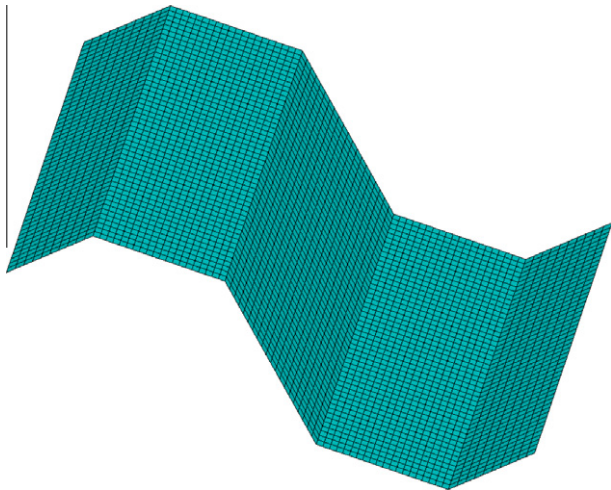
Fig. 2. The detailed finite element model for one period of a trapezoidal corrugated panel.

4. Numerical examples

The proposed equivalent stiffness properties are now compared to results from the literature, and also to detailed finite element models, to determine their effectiveness.

4.1. Trapezoidal corrugation

The first example is taken from Samanta and Mukhopadhyay (1999), based on an isotropic sheet material. The following properties for the standard trapezoidal corrugation profile are used

$$E = 21 \text{ GPa}, \quad v = 0.3, \quad b = 1.016 \text{ m}, \quad c = 0.0508 \text{ m},$$
$$f = 0.0127 \text{ m}, \quad t = 0.00635 \text{ m}, \quad \alpha = 45°.$$

The first stage is to determine the equivalent orthotropic plate properties. Table 5 shows the comparison of the proposed method with the orthotropic properties of Samanta and Mukhopadhyay (1999). To verify these properties, a detailed finite element model (FEM) for one period of the corrugation was constructed using ANSYS (ANSYS, 2011). Fig. 2 shows the mesh of the finite element model, which has 4131 nodes and 4000 SHELL63 elements. Bound-
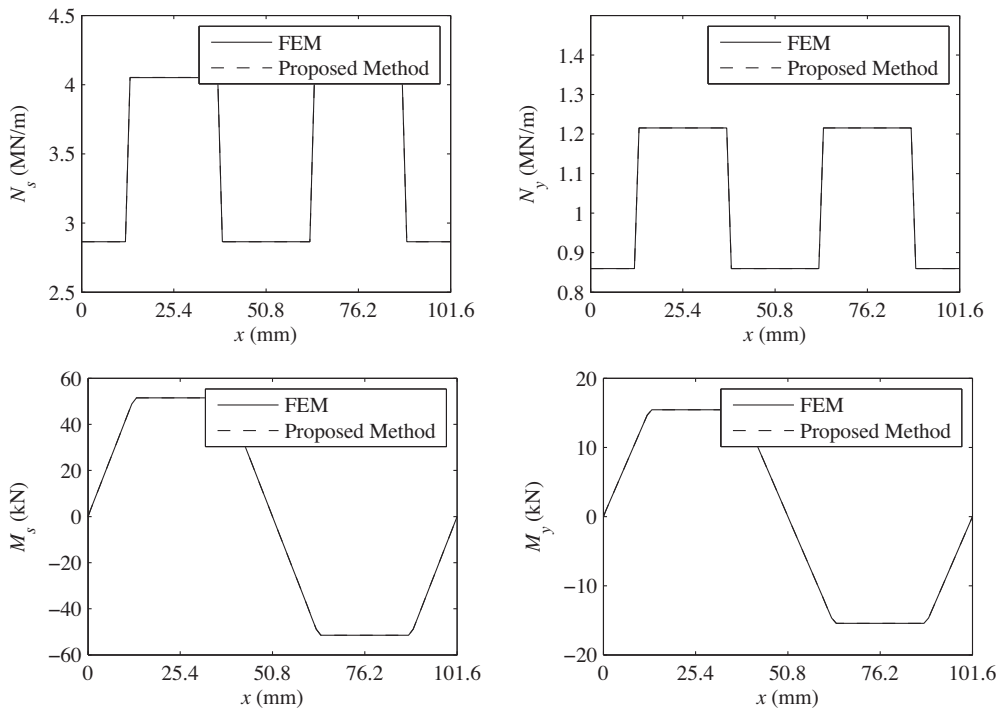

Fig. 3. Internal forces and moments for case 1.
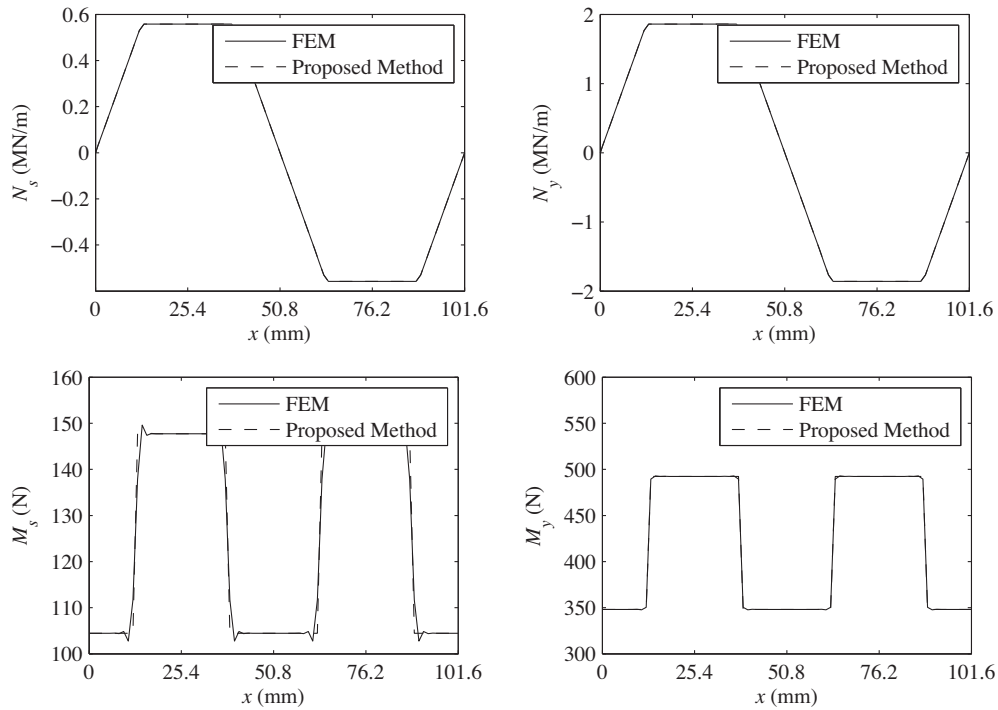
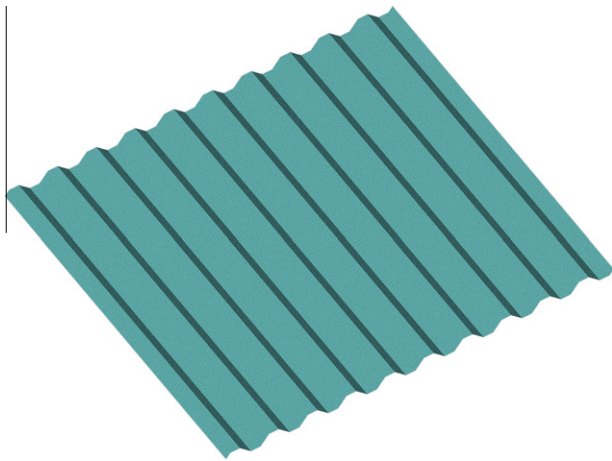Fig. 4. Internal forces and moments for case 5.

Fig. 5. A detailed finite element model for a panel constructed with trapezoidal corrugations.

Fig. 6. The displacement in the x–z and y–z planes for a panel constructed with trapezoidal corrugations.

ary conditions equivalent to those in Table 1 were applied to the finite element model, and the forces and moments at the boundaries used to calculate the equivalent properties. Table 5 also shows the finite element results and shows that the proposed method is very accurate, and produces a superior equivalent model to that of Samanta and Mukhopadhyay (1999).

The accuracy of the equivalent model is investigated further by comparing the internal forces and moments for two typical cases, namely case 1 and case 5, that are shown in Figs. 3 and 4. Clearly the internal forces and moments given by the proposed method are remarkably close to those given by the FEM. Thus our assumptions about the distribution of the internal forces and moments is reasonable.

The accuracy of the equivalent model should also be verified for a typical application. Here we consider a corrugated panel with 10 corrugation periods. The length of the corrugated panel in the x
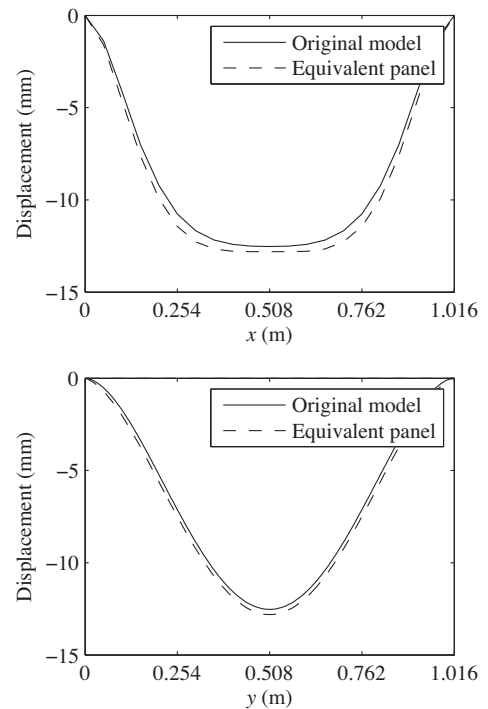
direction varies according to the number of corrugations, n. In this case, $n = 10$ and hence $a = 2c \times 10 = 1.016$ m. Fixed boundary conditions are assumed at each edge. The trapezoidal corrugated sheet is subject to a uniform distributed load of intensity equivalent to 69 kN/m^2. The panel has been analysed by a detailed shell model using ANSYS with 71655 nodes and 71120 SHELL63 elements, shown in Fig. 5, and also an equivalent orthotropic plate

Table 6
Material properties of AS4/3501-6.

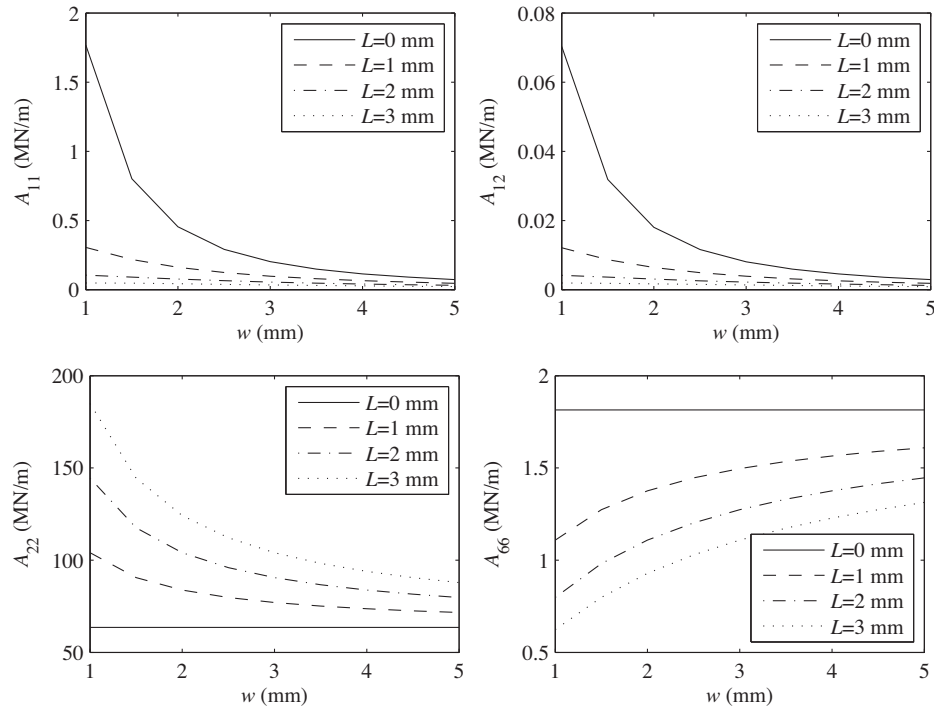| Axial modulus E_1 (GPa)	Transverse modulus E_2 (GPa)	Poisson's ratio v_{12}
148	10.5	0.3
Poisson's ratio v_{23}	Shear modulus G_{12} (GPa)	Shear modulus G_{23} (GPa)
0.59	5.61	3.17

Fig. 7. Variation of the in-plane stiffness for the round corrugation with $L = 0$, 1, 2 and 3 mm.
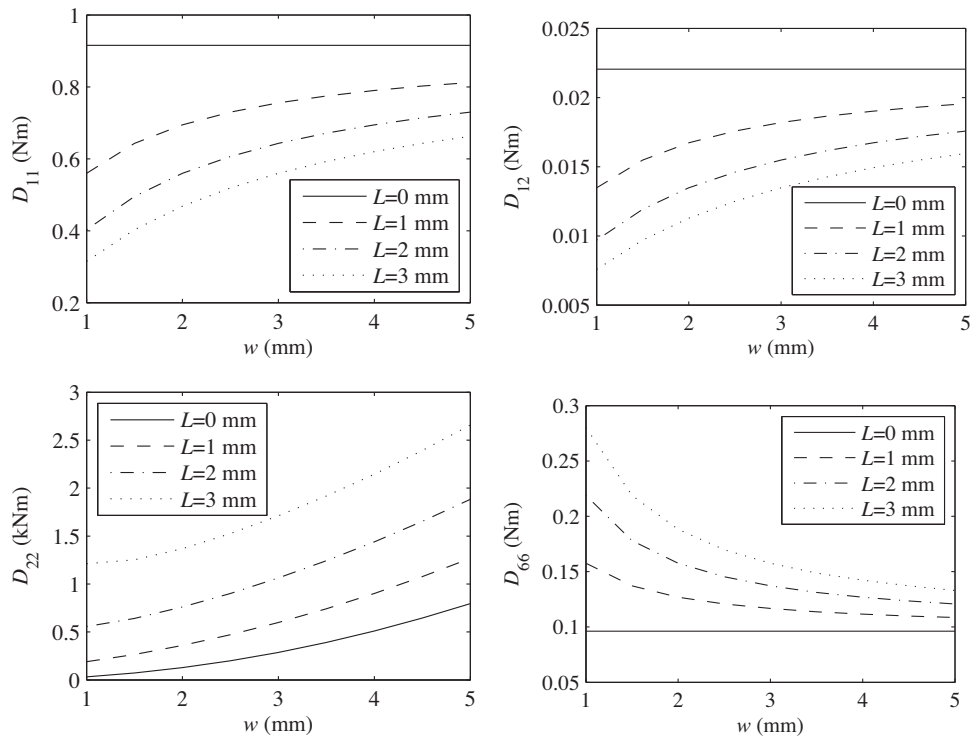

Fig. 8. Variation of the out-of-plane stiffness for the round corrugation with $L = 0$, 1, 2 and 3 mm.

Table 7
Stiffness properties for the example round corrugation.

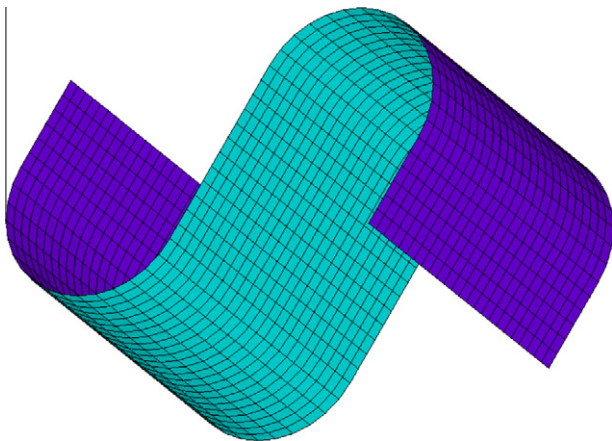|	Proposed method	Yokozeki et al. (2006)	FEM	Error (%) Proposed method vs. FEM
$\overline{A}_{11}$ (kN/m)	34.055	34.078	34.096	0.12
$\overline{A}_{12}$ (kN/m)	1.354		1.354	0.001
$\overline{A}_{22}$ (MN/m)	103.998	104.163	103.998	0.00
$\overline{A}_{66}$ (MN/m)	1.109		1.117	0.78
$\overline{D}_{11}$ (Nmm)	559.466	559.466	561.088	0.29
$\overline{D}_{12}$ (Nmm)	13.472		13.474	0.02
$\overline{D}_{22}$ (kNm)	1.710	1.710	1.711	0.017
$\overline{D}_{66}$ (Nmm)	157.558		157.581	0.015

Fig. 9. A detailed finite element model for a single round corrugation, for $R = L = 3$ mm.

model. Fig. 6 shows the deformation of the example panel both along and orthogonal to the corrugations, and compares the displacements estimated from the detailed finite element model with those from the proposed homogenised model. The displacements are quite close although the detailed finite element model is slightly stiffer than the equivalent model. The discrepancies are due to the fixed boundary conditions along the corrugated edge, since the equivalent model is not able to account for the stiffening effect of this boundary.

4.2. Round corrugation

In this case, the round-corrugation panel is made of AS4/3501-6 Carbon/Epoxy laminate, whose properties are given in Table 6. The ply angles are $[0/90]_s$. Figs. 7 and 8 show the predicted in-plane and out-plane stiffness of the corrugated composite as a function of the corrugated shape parameters, the corrugation period $w = 4R$ and length L. Table 7 shows a comparison between the proposed method and that of Yokozeki et al. (2006) for the particular case when $R = 3$ mm and $L = 3$ mm. This case is also modelled with the detailed finite element model shown in Fig. 9 for $b = 15$ mm and the results are also shown in Table 7. In this case, 1425 nodes and 1344 SHELL181 elements were used for the FEM estimation using ANSYS. The percentage difference between the results from the proposed method and the finite element model is also given and shows that the proposed method works well.

5. Conclusion

In this paper, an homogenisation-based analytical model, which is suitable for any corrugation shape, is presented. The previous methods usually require the original sheet material to be isotropic or to be treated as isotropic; in contrast, the method presented in this paper has no limitation in this regard. Furthermore, the coupling stiffnesses are also considered in the proposed method. The stiffness of the equivalent corrugated panel is obtained from the geometry of a unit-cell and the stiffness properties of the original sheet, which is convenient for the optimal design of morphing skins. The panel has been treated both as an original corrugated model and as an equivalent orthotropic model. Two numerical examples illustrated the validity of the proposed method, shown by the comparison of the results between the two approaches.

Parametric studies are planned to investigate the effects of corrugation geometry, ply angles, laminate thickness, fibre volume fraction, and so on. In addition the equivalent properties are simple functions of parameters determining the corrugation geometry. This is vital to incorporate the models into system models for conceptual design optimisation of morphing wing systems and is the subject of ongoing investigation.

References

Allaire, G., 2001. Shape Optimization by the Homogenization Method. Springer-Verlag, New York.

Andrianov, I.V., Bolshakov, V.I., Danishevs'kyy, V.V., Weichert, D., 2008. Higher order asymptotic homogenization and wave propagation in periodic composite materials. Proceedings of the Royal Society A, Mathematical, Physical and Engineering Sciences 464, 1181–1201.

ANSYS, 2011. Computer Software, version 13.0. <http://www.ansys.com/products/ansys13-new-features.asp>.

Barbarino, S., Bilgen, O., Ajaj, R.M., Friswell, M.I., Inman, D.J., 2011. A review of morphing aircraft. Journal of Intelligent Material Systems and Structures 22 (9), 823–877.

Bendsoe, M., Kikuchi, N., 1998. Generating optimal topologies in structural design using a homgenization method. Computer Method in Applied Mechanics and Engineering 71, 197–224.

Briassoulis, D., 1986. Equivalent orthotropic properties of corrugated sheets. Computers & Structures 23 (2), 129–138.

Gonella, S., Ruzzene, M., 2008. Homogenization and equivalent in-plane properties of two-dimensional periodic lattices. International Journal of Solids and Structures 45 (10), 2897–2915.

Kress, G., Winkler, M., 2010. Corrugated laminate homogenization model. Composite Structures 92 (3), 795–810.

Kress, G., Winkler, M., 2011. Corrugated laminate analysis: A generalized plane-strain problem. Composite Structures 93 (5), 1493–1504.

Liew, K.M., Peng, L.X., Kitipornchai, S., 2007. Nonlinear analysis of corrugated plates using a FSDT and a meshfree method. Computer Methods in Applied Mechanics and Engineering 196 (21-24), 2358–2376.

McFarland, D.E., 1967. An investigation of the static stability of corrugated rectangular plates loaded in pure shear. Ph.D. thesis, University of Kansas, Lawrence, KS.

Michel, J.C., Moulinec, H., Suquet, P., 1999. Effective properties of composite materials with periodic microstructure: a computational approach. Computer Methods in Applied Mechanics and Engineering 172, 109–143.

Miehe, C., Schotte, J., Lambrecht, M., 2002. Homogenization of inelastic solid materials at finite strains based on incremental minimization principles. application to the texture analysis of polycrystals. Journal of the Mechanics and Physics of Solids 50 (10), 2123–2167.

Miehe, C., Schotte, J., Schröder, J., 1999. Computational micro–macro transitions and overall moduli in the analysis of polycrystals at large strains. Computational Materials Science 16, 372–382.

Pellegrino, C., Galvanetto, U., Schrefler, B.A., 1999. Numerical homogenization of periodic composite materials with non-linear material components. International Journal for Numerical Methods in Engineering 46, 1609–1637.

Peng, L.X., Liew, K.M., Kitipornchai, S., 2007. Analysis of stiffened corrugated plates based on the FSDT via the mesh-free method. International Journal of Mechanical Sciences 49 (3), 364–378.

Ruzzene, M., Baz, A., 2000. Control of wave propagation in periodic composite rods using shape memory inserts. Journal of Vibration and Acoustics 122, 151–159.

Saavedra Flores, E.I., de Souza Neto, E.A., 2010. Remarks on symmetry conditions in computational homogenisation problems. Engineering Computations 27 (4), 551–575.

Saavedra Flores, E.I., de Souza Neto, E.A., Pearce, C., 2011. A large strain computational multi-scale model for the dissipative behaviour of wood cell-wall. Computational Materials Science 50 (3), 1202–1211.

Samanta, A., Mukhopadhyay, M., 1999. Finite element static and dynamic analysis of folded plates. Engineering Structures 21, 277–287.

Smith, D.D., Isikveren, A.T., Ajaj, R.M., Friswell, M.I., 2010. Multidisciplinary design optimization of an active nonplanar polymorphing wing. In: 27th Congress of the International Council of the Aeronautical Sciences, 19–24 September 2010, Nice, France.

Suquet, P., 1993. Overall potentials and extremal surfaces of power law or ideally plastic materials. Journal of the Mechanics and Physics of Solids 41, 981–1002.

Thill, C., Etches, J.A., Bond, I.P., Potter, K.D., Weaver, P.M., 2008a. Morphing skins - a review. The Aeronautical Journal 112, 117–139.

Thill, C., Etches, J.A., Bond, I.P., Weaver, P.M., Potter, K.D., 2008b. Experimental and parametric analysis of corrugated composite structures for morphing skin applications. In: 19th International Conference on Adaptive Structures Technology, 6–9 October 2008, Ascona, Switzerland.

Thill, C., Etches, J.A., Bond, I.P., Potter, K.D., Weaver, P.M., 2010a. Composite corrugated structures for morphing wing skin applications. Smart Materials and Structures 19, 124009.

Thill, C., Etches, J.A., Bond, I.P., Potter, K.D., Weaver, P.M., Wisnom, M.R., 2010b. Investigation of trapezoidal corrugated aramid/epoxy laminates under large tensile displacements transverse to the corrugation direction. Composites Part A - Applied Science and Manufacturing 41 (1), 168–176.

Wellmann, C., Wriggers, P., 2008. Comparison of the macroscopic behavior of granular materials modeled by different constitutive equations on the microscale. Finite Elements in Analysis and Design 44, 259–271.

Winkler, M., Kress, G., 2010. Deformation limits for corrugated cross-ply laminates. Composite Structures 92 (6), 1458–1468.

Xia, Y., Friswell, M.I., 2011. Equivalent models of corrugated laminates for morphing skins. In: Ghasemi-Nejhad, M.N. (Ed.), Proceedings of SPIE, Active and Passive Smart Structures and Integrated Systems, vol. 7977. San Diego, USA.

Yokozeki, T., Takeda, S.-I., Ogasawara, T., Ishikawa, T., 2006. Mechanical properties of corrugated composites for candidate materials of flexible wing structures. Composites: Part A 37, 1578–1586.